Deep Learning-Enhanced ANFIS Classifier for Solar Panel Image Analysis

M. Perarasi[1]* B.Sarala[2], S. Anita[3], Chairma Lakshmi K R[4]

[1&2] Associate Professor,Department of Electronics and Communication Engineering,

[3] Associate Professor, Department of Electrical and Electronics Engineering,

[4] Associate Professor, Department of Electronics and Instrumentation Engineering,

[1,2,3,4] R.M.K. Engineering College, Tamil Nadu, India.

*[1] to whom all correspondence should be addressed: E-mail: arasi.angel@gmail.com

[2]saralailangovan@gmail.com, [3]saa.eee@rmkec.ac.in,[4]chermalakshmi@gmail.com

Graphical Abstract

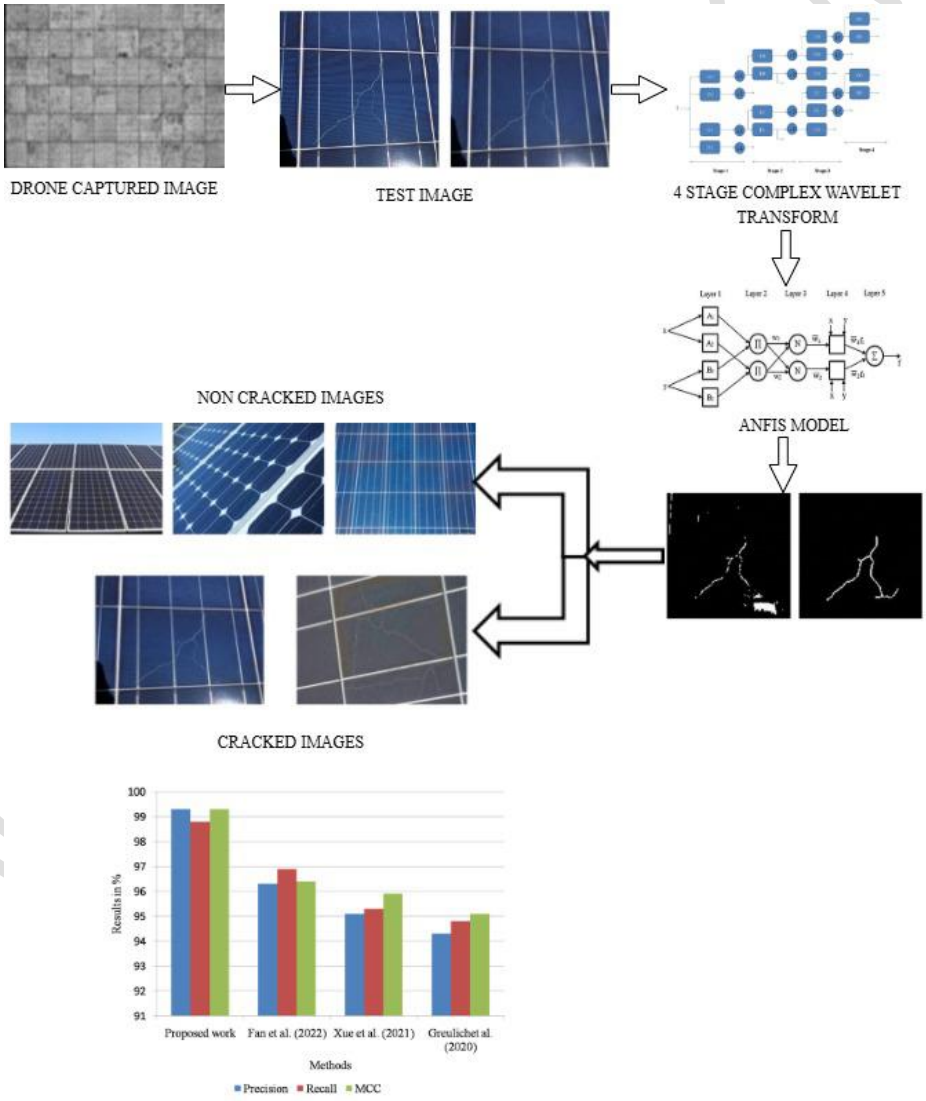

Abstract

Electricity demand is increasing day by day and hence power utilities are slowly shifting towards renewable energy, mainly solar, as it is more reliable and environment friendly. However, solar power generation systems have very low efficiency and this is the major challenge faced by the researchers. Some of the reasons for the low efficiency is the presence of dust particles, bird droppings, shadows, rain droplets, micro cracks etc. Micro cracks are the major issue to reduce solar panel efficiency. Microcracks are estimated to contribute to a power loss of approximately 80–90%, severely affecting the efficiency and overall performance of solar panels.In this article, the cracked panel and non-cracked panel can be identified by using complex wavelet transform. The Gaussian filter is used to eliminate the distortions in the cracked panel. And this image can be decomposed by sub band images. The corresponding statistical and texture features can be calculated for sub band images and these features are classified using ANFIS classifier. Finally the segmentation algorithm is used to detect the cracked and non-cracked panel images. By comparing with existing methods like Electroluminescence imaging technique, ResNet152 model, Xception model, UAV based thermal imaging technique. The Proposed ANFIS leverages the advantages of both neural networks and fuzzy logic, enhancing the accuracy and adaptability in distinguishing cracked from non-cracked panels. This approach can be deployed in automated inspection systems for large-scale solar farms, enabling early crack detection. By identifying issues sooner, it helps lower maintenance costs while improving the efficiency and longevity of solar panels. Additionally, the method can be integrated with drone-based monitoring systems for remote inspections.

Keywords: ANFIS classifier, Machine Learning, complex Wavelet Transform

1. Introduction

Micro cracks are mainly due to manufacturing defects as well as improper handling during transportation and installation. Manual testing of panels for the detection of micro cracks is very difficult and time consuming especially for panels of large dimensions and high-power rating. For precise fractures being identified, image quality is essential. If the image resolution is inadequate, surface sounds could be mistaken for cracks. As a consequence, a minimum pixel range needs to be defined to perform the function correctly. Careful algorithm selection is crucial to the process' accuracy since it produces a model that performs better and has greater identifying potential. An examination of research revealed that soft computing methods fared better in terms of precision than other methods. Some methods for the automated detection of cracks are available in the literature. The performance

metrics of these methods along with the time taken for the detection of cracks is also available in the literature. This work addresses the process of detection of micro cracks using an improved technology which detects the crack within very less time as compared to the existing technologies. If the cracks in the solar panels are detected using automated methods, it becomes easier to change the defected panel with a new one so as to improve the production rate. This paper deals with ANFIS machine learning algorithm as a soft computing technique to detect the defective panel images.

2. Literature Survey

Deep learning (DL) models are used by some researchers for solar cell fracture detection. Improved EL detection of solar cell fractures is proposed by Su *et al.* (2021) by implementation of a unique complementary attention network. Out of 3629 photos tested by them almost 2129 have detective sections. 2 to 12% of the output power may be lost because of these tractions and it depends on the dimensions of the cracks. The research shows that fractures also referred to as "cracks" in solar cells might diminish the cell's output power by anywhere from 0.9% to 42.8%, or even more. Li *et al.* (2014) have proposed an entirely new method for finding cracks in faults with dark colours and poor contrast. The original image is divided into its component parts and then recreated using the FDCT (Fast Discrete Curvelet Transform) technique. In order to remove surface textures from the images, constraints for the decomposition parameters are derived using texture feature measurements. Contours from the rebuilt images are obtained, which are free of motifs but contain fracture fault contours, to produce the required image. A method for spotting cracks in Scanning Electron Microscopy(SEM) images is described by Vidal *et al.* in (2016). They have merged the SEM pictures by setting an acceptable threshold defined by the image histogram after filtering out nodules and background noise. Image binarization is achieved to successfully detect fractures from the backdrop of the image. The spatial area of the fractures are more accurately determined by combining the second derivative of the histogram acquired using the Laplacian of Gaussian (LoG) with the Prewitt vertical edge detector. A method for locating near-surface faults in specimens that are both magnetizable and conductible is proposed by Heideklang *et al.* (2015). Their approach integrates information from thermography, magnetic flux leakage, and eddy current testing. For pixel-level fusion of data, a variety of signal processing methods are provided to normalise the information. The signal-level fusing of disparate Non-Destructive Testing (NDT) image results are achieved utilising pixel-wise, multi-scale, and signal

normalisation methods. Fundamental algebraic fusion techniques are used to combine the findings of signal normalisation. Zahra Anvari and Vassilis Athitsos *et al*.(2021) The deep learning techniques used for document picture enhancement tasks, such as binarization, deblurring, denoising, defading, watermark removal, and shadow removal, are thoroughly reviewed in this work. The authors identify difficulties and constraints and offer potential avenues for further research while discussing the different deep learning architectures, datasets, and metrics employed in these tasks. Muhammad Imran Razzak, Saeeda Naz, and Ahmad Zaib (2017) This paper presents an overview of deep learning architectures and their optimization techniques used in medical image segmentation and classification. It discusses the unique challenges faced in medical image processing and outlines open research issues, emphasizing the potential of deep learning to improve healthcare services.

The novelties of this proposed solar panel crack detection system are constructed from the literature survey section and they are highlighted in the below points.

- The novel ANFIS Classifier is proposed in this work to perform the solar panel image classification process.
- The novel crack segmentation algorithm is proposed in this work model.

The generic procedure for the image processing technique is shown in the Figure 1.

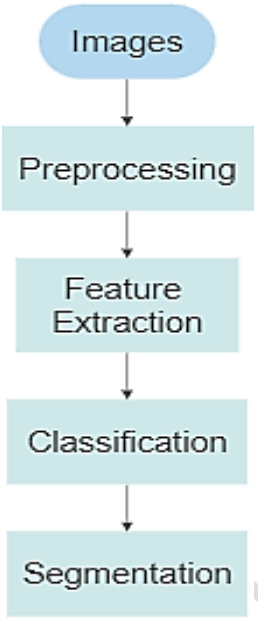

Figure 1 Generic Procedures for Image Processing

3. Proposed Methodologies

In this paper ANFIS classification method used in the panel and divided like cracked and Non-cracked panels. The Gaussian filter is applied and the noise removed. By using image processing technique the panel can be separated by cracked and Non-cracked panels.The proposed block diagram is given below in Figure 2.

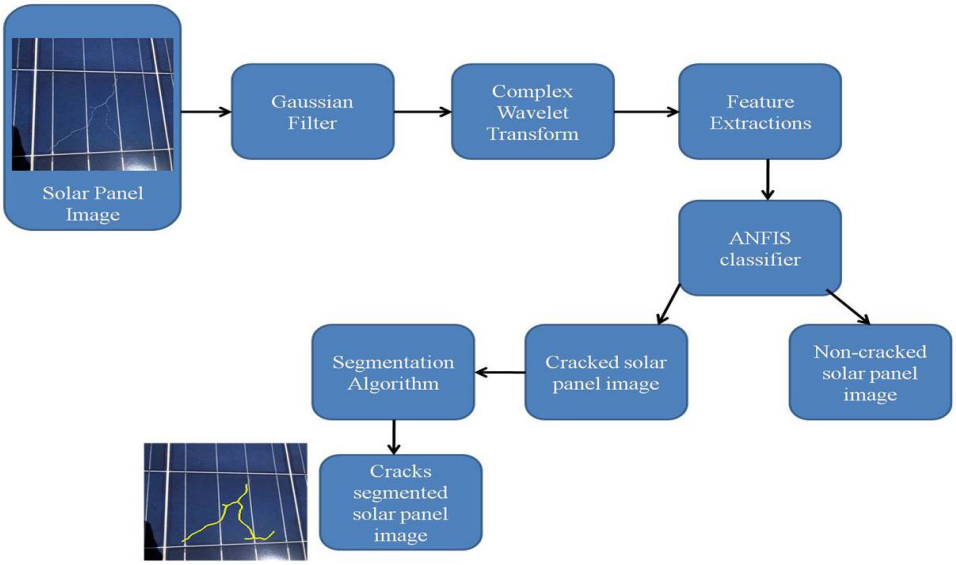

Figure 2 ANFIS classifier based solar panel image classification scheme

Table 1 shows that training and testing dataset values and Detection Rate values.

Panel Type	Training Dataset	Testing Dataset	Detection Rate
Cracked Panel	285	665	99.8%
Non-cracked Panel	300	700	98.4%

Table 1 Training and Testing Dataset

In this work, MATLAB 2020 is used here as simulation platform on computer with the following specifications.

Processor : Intel i5

Hard disk : 2 TB

RAM : 8 GB RAM.

3.2.1 Optical System Specifications

Here, FIMI X 8 drone is utilized to take pictures of the solar arrays. The camera on the drone can rotate in three axes and has a catching range of up to five thousand meters. Drone camera units weigh 790 grams, and they can transmit data at 64 km per hour. The optical system employed in this study is characterized by its resolution and optical transfer properties. The optical system of this research makes use of various kinds of photo detectors. The drone instrument's optical system takes pictures of the solar panels. The qualities of the object being tested may be determined without physically touching it due to the optical measuring procedures. This method uses the physics of absorption and reflection to record information about surfaces as a whole. The drone instrument has a variety of optical components and assemblies, all of which must be meticulously constructed for optimal image performance. When designing optical components, it is common practice to strive for the smallest feasible footprint in terms of size, weight, and energy consumption. Drones and other autonomous systems may have their lenses made from a wide variety of substrates, including plastic, glass, metal, and plastic. UAV applications that collect distant pictures need long focus lengths. However, this viewpoint results in a deformed picture; to fix this, the perspective image registration approach is employed.

Figure 3 (a) depicts the original picture recorded, whereas Figure 3 (b) shows the rectified image after preprocessing. The resulting solar panel pictures are registered using the feature image registration approach described by Wang *et al.* (2022).

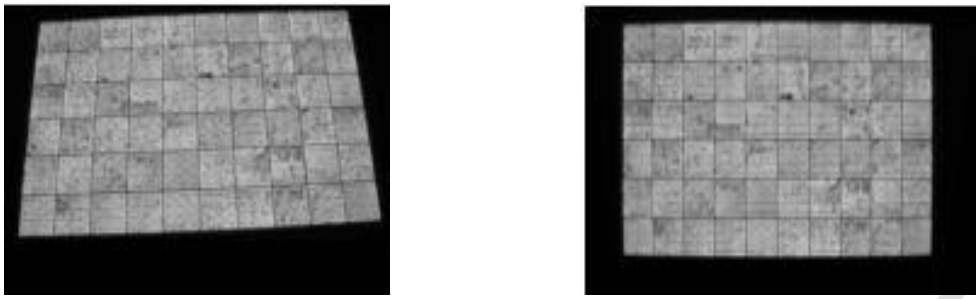

(a) **(b)**

Figure 3 (a) Image captured by using Drone (b) Registered image

The licensed solar panel picture has six rows of ten solar cells, every single one of which measures 0.16 m X 0.16 m.

3.2.2 Preprocessing

The extracted picture of the solar panel suffers from blurring in the broken areas, which in turn affects the clarity of the individual pixels. These unnecessary blurs should be eliminated so that fractured spots in solar panels may be detected and segmented. Even though many conventional blur detection methods as stated in Awais Khan *et al.* (2021) and Renting Liu *et al.* (2008) available to detect and remove the blur from the solar images, these methods exhibits pixel losses during deblur process. The Data Augmentation Methods (DAM) is used in the solar panel images of the training data set to increase the number of solar panel images during the training of the ANFIS classifier. This work uses left shift and right shift DAM methods in the training dataset solar panel images.

The 'Gaussian' filter, whose response to impulses is a Gaussian function, is used to identify and get rid of the blurry pixels in the solar cell picture. The formula below represents the kernel of the Gaussian filter given in the Equation (1)

$$G(r,s) = \frac{1}{\sqrt{2\pi}\sigma} e^{\frac{-r^2+s^2}{2\sigma^2}} \quad (1)$$

The filter has a mean of zero and a window size of 5 X 5, hence the standard deviation is zero. To identify and eliminate the haze around the cracks in the solar cell, a Gaussian filter is used in the picture. The original picture of the solar panels is shown in Figure 4 (a), while the filtered version is shown in Figure 4 (b).

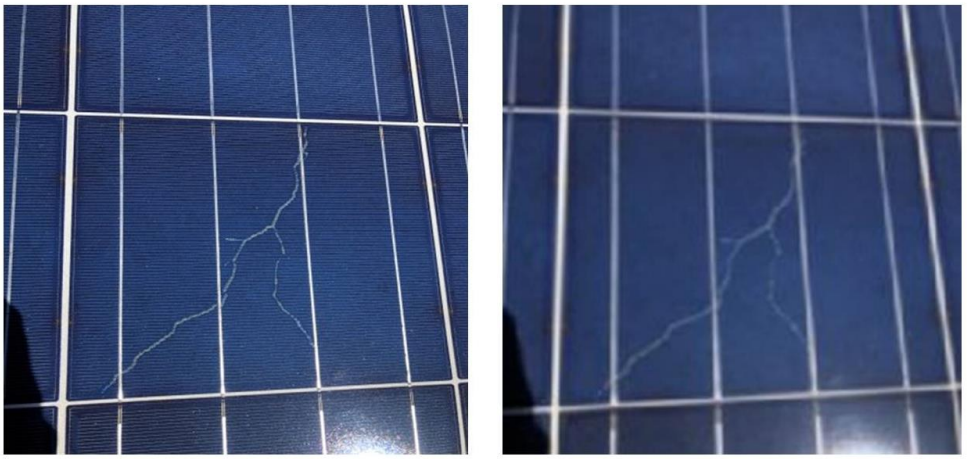

(a) **(b)**

Figure 4 (a) Source solar panel image (b) Gaussian filtered image (Pre-processed image)

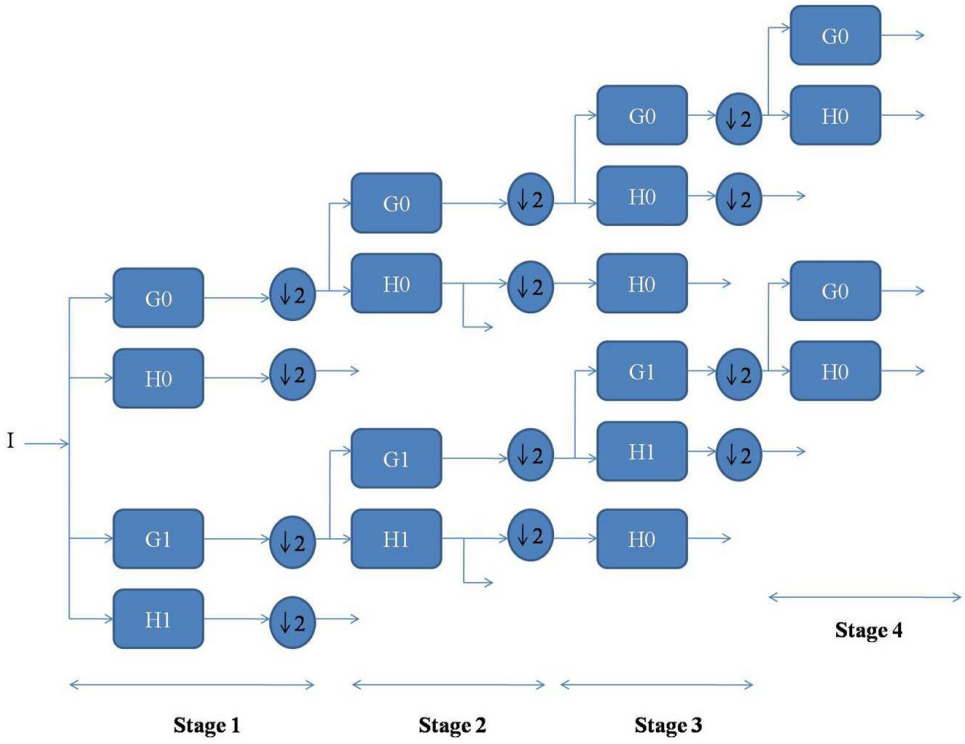

Figure 5 Four stage Complex Wavelet Transform

The picture may be decomposed into smaller scales using CWT. This study uses a 4-stage CWT to separate the solar panel picture into 12 individual sun band images. The suggested CWT is made up of two filters with four phases each: a Low Pass Filter (G) and a High Pass Filter (H). At each step of the disintegration, the input picture is concurrently processed by these filter banks to generate the sub spectrum images. The output of each step is down filtered by a factor of 2, as shown in Figure 5.

In a CWT structure, real and scaling properties are given in the Equations (2) and (3) respectively.

$$\emptyset(t) = \sqrt{2}\sum \quad G0\emptyset(2t-n) \tag{2}$$

$$\vartheta(t) = \sqrt{2}\sum \quad G1\emptyset(2t-n) \tag{3}$$

The CWT structure's high pass filter banks' real valued function and scaling function are given in the Equations (4) and (5) respectively.

$$\emptyset(t) = \sqrt{2}\sum \quad H0\emptyset(2t-n) \tag{4}$$

$$\vartheta(t) = \sqrt{2}\sum \quad H1\emptyset(2t-n) \tag{5}$$

Figure 6 shows the pre-processed solar panel picture broken down into 12 sub band images. The statistical and texture features can be computed for all the sub band images.

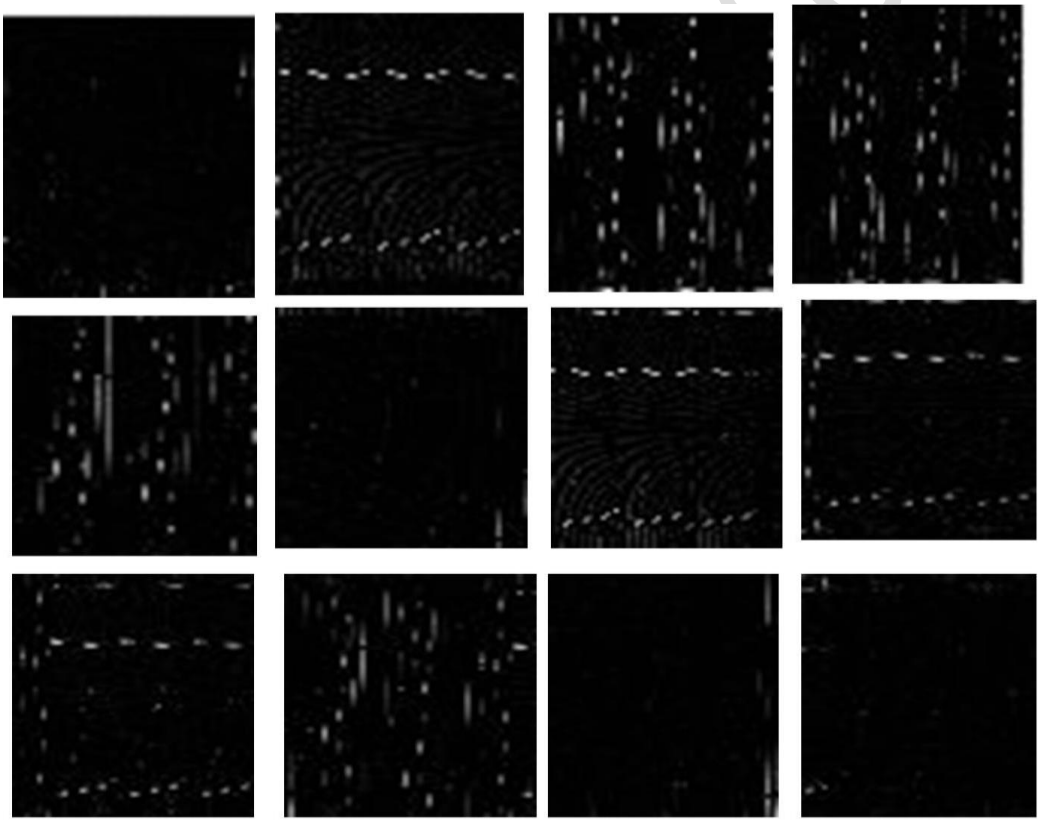

Figure 6 DTCWT sub band images

3.2.4 Computation of Features

Pixels in a picture may be distinguished from one another based on their features, which are their unique characteristics. CWT is used to split pictures into sub bands before

computing texture and statistical information from those images. The next sections elaborate on these aspects.

Statistical features

These characteristics use the coefficient fluctuations and their mean value in each decomposed sub band picture to differentiate between images of cracked and uncracked solar panels.

Mean

The following formula is used to get the average value of each sub band picture.

$$Mean(\underline{C}) = \frac{\sum_{i=1}^{N} C_i}{N} \quad (6)$$

In this equation, N represents the total number of coefficients in the decomposed sub band picture, and C_i represents the coefficients of image

Variance

Decomposed sub band images have somewhat distinct coefficients from one another. The variance functions allow for the estimation of these differences. Each sub band image's variance is calculated separately using the following formula.

$$Variance = \frac{\sum_{i=1}^{N} (C_i - \underline{C})^2}{N} \quad (7)$$

Skewness

Skewness characteristics, which are calculated using a third-order functional factor, characterize the form and size of the deconstructed sub band picture. Each sub band image's Skewness level may be calculated using the following formula.

$$Skewness = \frac{1}{N}\sum_{i=1}^{N} \left[\frac{C_i - \underline{C}}{\sigma}\right]^3 \quad (8)$$

Kurtosis

Kurtosis characteristics, which are calculated using a fourth-order functional factor, characterise the non-linear behaviour of each coefficient in a sub-band picture. Using the following formula, the kurtosis of each individual sub band picture is obtained.

$$kurtosis = \frac{1}{N}\sum_{i=1}^{N} \left[\frac{C_i - \underline{C}}{\sigma}\right]^4 \quad (9)$$

Pearson's Index

For each picture sub-band, Pearson's index is calculated based on its skewness and kurtosis. The formula that follows is used to get the Pearson's index applying the Skewness feature.

$$Pearson's\ SkewnessIndex\ (PSI) = \frac{\underline{C}}{Skewness - Variance} \quad (10)$$

The formula that follows is used to get the Pearson's index utilizing the Kurtosis characteristic.

$$Pearson's\ KurtosisIndex\ (PKI) = \frac{\underline{C}}{Kurtosis - Variance} \quad (11)$$

Texture features

One alternative name for textures is patterns. Images of fractured solar panels have a distinct texture that is not present in images of undamaged solar panels. Therefore, it is crucial for the classification procedure to compute the textures of each deconstructed sub band picture. The following texture characteristics are calculated from each sub band image's decomposition.

$$Energy = \sum_{i,j} \quad f(i,j)^2 \tag{12}$$

Each deconstructed picture may be reconstructed by computing the texture matrix (rows and columns are denoted as i and j) using the formula:

$$Correlation = \sum_i \quad \sum_j \quad \frac{(i-\mu_i)(j-\mu_j)f(i,j)}{\sigma_i \times \sigma_j} \tag{13}$$

where,

$$\mu_i = \sum_i \quad i \sum_j \quad f(i,j)$$

$$\mu_j = \sum_j \quad j \sum_i \quad f(i,j)$$

$$\sigma_i = \sum_i \quad (i-\mu_i)^2 \sum_j \quad f(i,j)$$

$$\sigma_j = \sum_j \quad (j-\mu_j)^2 \sum_i \quad f(i,j)$$

$$Inertia = \sum_{i,j} \quad (i-j)^2 f(i,j) \tag{14}$$

$$ClusterShade = \sum_{i,j} \quad \left[(i-\mu_i) + \left(j-\mu_j\right)\right]^3 f(i,j) \tag{15}$$

$$ClusterProminence = \sum_{i,j} \quad \left[(i-\mu_i) + \left(j-\mu_j\right)\right]^4 f(i,j) \tag{16}$$

$$Homogeneity = \sum_{i,j} \quad \frac{1}{1+(i-j)^2} f(i,j) \tag{17}$$

$$Contrast = \frac{1}{(N-1)^2} \sum_{i,j} \quad (i-j)^2 f(i,j) \tag{18}$$

where, N is the element counts in $f(i,j)$.

4. ANFIS Classification Technique

It is the classification of calculated characteristics for broken solar panel detection. Researchers have employed a variety of machine learning methods, including the Support Vector Machine (SVM) and the binary classification algorithm, to identify solar panels with cracks. Using these Machine Learning (ML) techniques to identify damaged panels is insufficient. In this study, the ANFIS classification architecture is developed for differentiating between images of damaged and non-cracked solar panels. The designed ANFIS structure has two modes of operation: training and testing. The ANFIS classifier learns using a feature matrix that contains information on each picture in the training dataset, organized by the bands in which they were taken. The ANFIS architecture's binary index is generated at the testing level. The ANFIS classification framework returns a value of '1' if it is defect one and a value of '0' otherwise. In Figure 6, the ANFIS architecture developed for this study is shown. Layer 1 nodes A and B are associated with the classification nodes and the Layer 2 performs inbuilt multiplication work and its nodes are identified by the label. This layer conducts the process of multiplication of the previous layer output. The weights calculated in preceding layers are used as input to Layer 3, where they are normalized by calculating their mean. N stands for the nodes in this layer. In Layer 4, fuzzy rules are incorporated with the nodes laid here and defuzzification process is performed here. The output is the result of layer 5's summing function, which sums the answers from the preceding layers. The ANFIS classification structure is shown in Figure 7 (a) and Figure 7 (b) depicts pictures of defected and non-defected solar panel PVs, respectively.

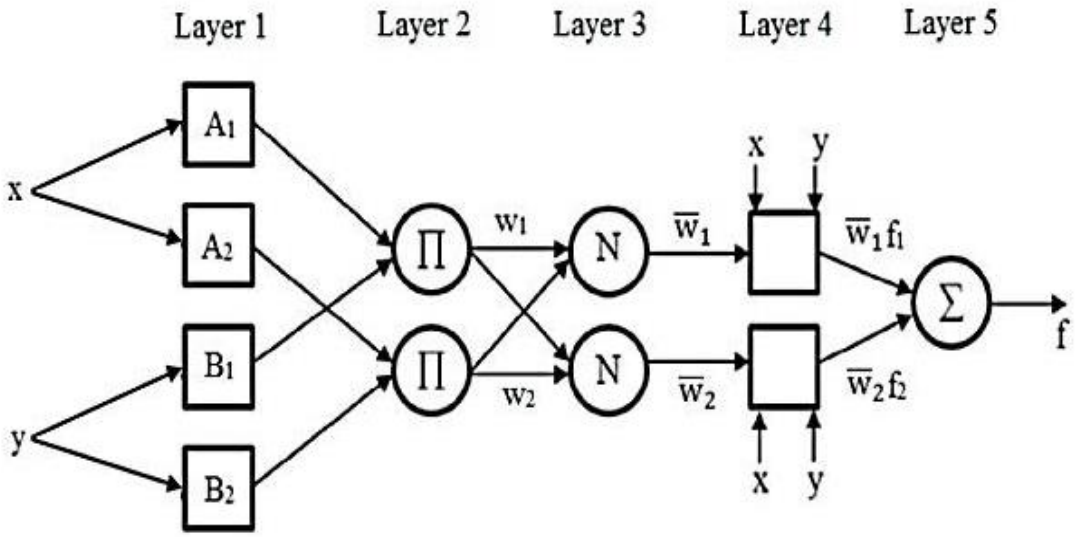

Figure 7 Architecture of ANFIS model

(a)

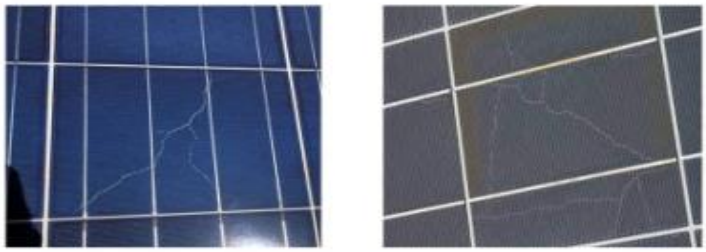

(b)

Figure 8 (a) Non-defected PV images (b) Defected PV images

5. Segmentation Algorithm

Crack segmentation algorithm is the method used to separate apart the shattered areas of the picture of the broken solar panel. The broken pixels may be found using the following approach.

Phase 1:

Suppressing the border-connected outlier pixel structure in the categorized fractured solar panel picture.

- Purpose: Removes noise from the edges of the image to prevent false detections.
- Impact on Accuracy: Reduces the chances of misclassifying background elements as cracks.
- Intermediary Result: Show an image before and after outlier removal.

Phase 2:

If the pixel's value is below 50, set it to Zero in the picture.

- Purpose: Eliminates low-intensity pixels (background noise), keeping only significant crack regions.
- Impact on Accuracy: Enhances contrast between the crack and background, making segmentation more reliable.
- Intermediary Result: Show an image where faint background noise is eliminated.

Phase 3:

In order to create the enlarged picture, use the dilation operator with the 'disc' structural element and a 13 mm radius.

- Purpose: Expands and connects broken crack segments.
- Impact on Accuracy: Helps in detecting complete cracks rather than fragmented parts.
- Intermediary Result: Compare an image before and after dilation to show how small gaps are filled.

Phase 4:

The enhanced picture should undergo the same steps as before.

- Purpose: Reinforces the dilation effect to ensure no crack is missed.
- Impact on Accuracy: Prevents under-segmentation, making sure all cracks are considered.
- Intermediary Result: Show how cracks are progressively becoming more distinct.

Phase 5:

Figure 7 (a) shows the eroded result of using an erosion operator with a 'disc' structural element and a 5 mm radius for generating erode image.

- Purpose: Reduces over-segmentation caused by dilation, retaining only meaningful crack structures.
- Impact on Accuracy: Eliminates falsely expanded regions, improving precision.
- Intermediary Result: Show a comparison where unwanted noise is removed.

Phase 6:

As shown in Figure 7 (b), the final crack area segmented picture is created by employing the 'thin' operator to convert the numerically degraded image into a logical image by removing pixels without holes.

- Purpose: Converts the processed image into a logical binary form while preserving essential crack features.
- Impact on Accuracy: Ensures that only relevant crack pixels remain, making detection more precise.
- Intermediary Result: Final segmented crack image with clear boundaries.

(a) **(b)**

Figure 9 (a) Eroded image (b) Crack segmented image

6 Results and Discussion

The algorithm stated in this article is tested on the real time constructed dataset solar panel images. This constructed dataset consists of 950 fractured solar panel images and 1000 non-fractured solar panel images. The solar panel image size is about 512 x 512 pixels as width and height. The proposed system splits the constructed dataset into 30:70 ratio for training and testing. Hence, the training solar panel image dataset consists of 285 fractured solar panel images and 300 non-fractured solar panel images. Similarly, the testing solar panel image dataset consists of 665 cracked solar panel images and 700 non-cracked solar panel images. The detection rate for cracked solar panel is 99.8% by correctly detecting 664 cracked solar panel images over 665 images. The detection rate for non-cracked solar panel is 98.4% by correctly detecting 689 cracked solar panel images over 700 images. Therefore, the mean detection rate is about 99.1%.

The performance of the ANFIS based solar panel defect system is evaluated using the following equations.

$$Sensitivity(Se) = \frac{TP}{TP+FN} \times 100\% \quad (19)$$

$$Specificity(Sp) = \frac{TN}{TN+FP} \times 100\% \quad (20)$$

$$Accuracy(Ac) = \frac{TP+TN}{TP+TN+FP+FN} \times 100\% \quad (21)$$

$$Precision(Pr) = \frac{TP}{TP+FP} \times 100\% \quad (22)$$

$$MCC = \frac{TP*TN-FP*FN}{\sqrt{(TP+FP)(TP+FN)(TN+FP)(TN+FN)}} \quad (23)$$

The correctly detected defected and non-defected images are TP and TN and the incrrectly detected defected and non-defected images are FP and FN respectively. The average values of 97.6% for Se, 97.6% for Sp, 98

Table 2 shows the comparisons of Data Augmentation Methods (DAM) results for both case of images.

Table 2 Comparisons of Data Augmentation Methods (DAM) results

Cases	Procedure analysis	DT Results in %
For cracked solar panel images	Proposed solar panel image classification incorporating DAM	97.33
	Proposed solar panel image classification without incorporating DAM	95.12
For cracked solar panel images	Proposed solar panel image classification incorporating DAM	98.6
	Proposed solar panel image classification without incorporating DAM	96.65

Table3 shows the index parameter analysis on solar panel image dataset. The proposed solar panel image classification system obtains 99.3% precision, 98.8% recall and 99.3% MCC. (Mathew Correlation Coefficient)

Table 3 Index parameter analysis

Index Parameters	Results in %
Precision	99.3
Recall	98.8
MCC	99.3

Figure 10 shows the graphical perspective of Index parameter analysis.

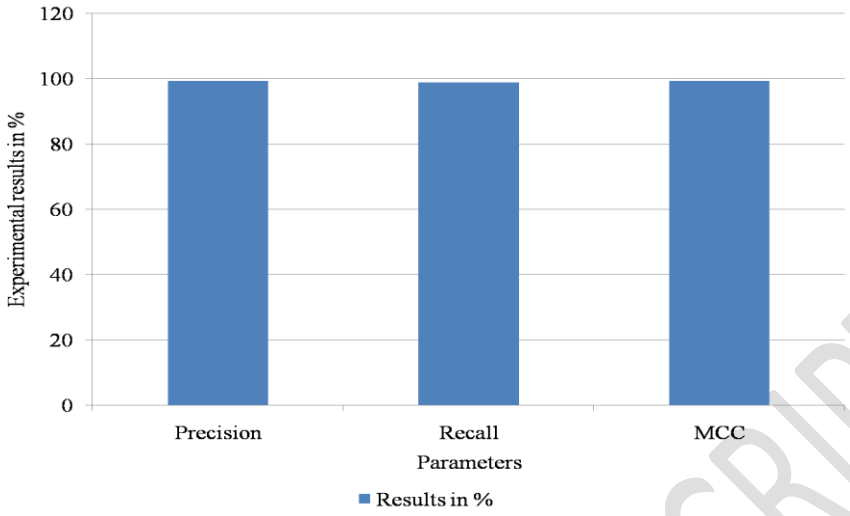

Figure 10 Graphical perspective of Index parameter analysis

Table 4 gives the comparative analysis of image classification system and the ANFIS classifier is used. It is observed that the results obtained from the proposed work are significantly improved in comparison with similar models proposed by Fan *et al*. (2022), Xue *et al*. (2021) and Greulich *et al*. (2020). The proposed solar panel classification system obtains 99.3% precision, 98.8% recall and 99.3% MCC using ANFIS classification approach.

Table 4 Comparative analysis for the solar panel image classification system

Methods	**In %**		
	Precision	**Recall**	**MCC**
Proposed ANFIS model	99.3	98.8	99.3
Fan *et al*. (2022)	96.3	96.9	96.4
Xue *et al*. (2021)	95.1	95.3	95.9
Greulich *et al*. (2020)	94.3	94.8	95.1

Figure 11 shows the graphical comparative analysis for the solar panel image classification system.

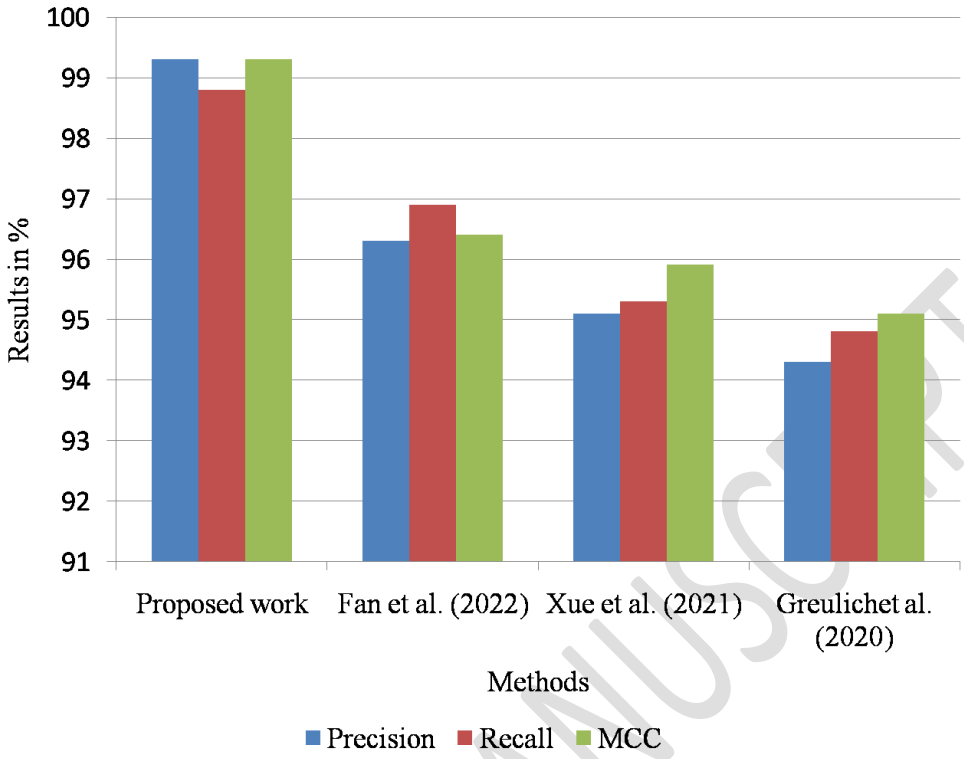

Figure 11 Graphical comparative analysis for the solar panel image classification system

The comparisons of SDT in automatic signal classification system are important because it gives ratio between the correctly detected case and the total case. Table 5 is the SDT(signal Detection Time) comparisons on BB dataset. The proposed solar panel classification system consumes 0.87 ms for classifying the single solar panel image.

Table 5 SDT comparisons on BB dataset

Methods	**SDT in ms (per signal)**
Proposed ANFIS	0.87
Fan *et al.* (2022)	1.76
Xue *et al.* (2021)	1.59
Greulich *et al.* (2020)	1.97

Figure 12 shows the graphical analysis of SDT comparisons on BB dataset.

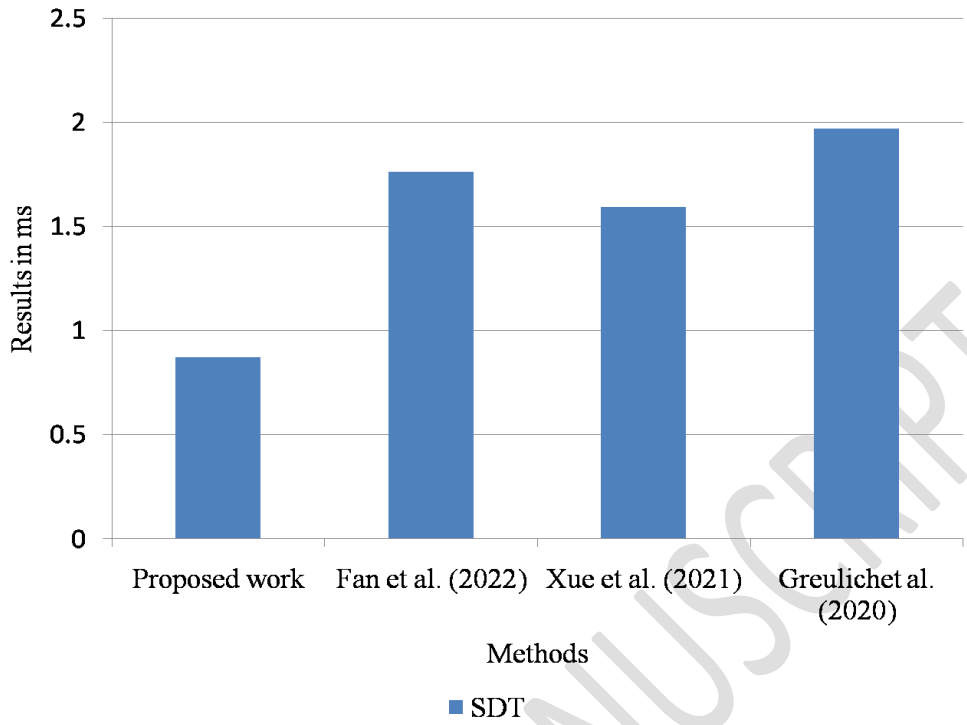

Figure 12 Graphical analysis of SDT comparisons on BB dataset

Validation of this results can be used by k-fold cross validation method with K=6 where 120 testing images are grouped with 20 images per fold. 75% of the 20 images are trained and 25 % are tested. The average accuracy is 98.2%

7. Conclusion

The ANFIS classifier based solar panel image detection and classification methods using CWT transform is presented. The proposed classification model detects and classifies the defected images using ANFIS architecture. The classification model was evaluated on a controlled dataset, and its resilience in real-world situations, such fluctuating lighting, dust deposition, or panel degradation, requires additional assessment. The existing methodology predominantly emphasizes fracture identification, whereas other defect types, including delamination, discolouration, and hotspots, might be integrated into the categorization process for a more thorough evaluation. Integrating this model into automated inspection systems utilizing drone-mounted cameras or industrial monitoring configurations could substantially improve solar panel maintenance. Future research may investigate hybrid models based on deep learning to enhance classification performance, alongside real-time deployment strategies for the effective management of large-scale solar farms. Then, the crack detection algorithm is used to classify fractured solar panel images

and Non-fractured panel images. The proposed solar panel classification system obtains 99.3% precision, 98.8% recall and 99.3% MCC using ANFIS classification approach. It consumes 0.87 ms for classifying a single solar panel image.

8. References

1. F. Haase, J. Käsewieter, S. R. Nabavi, E. Jansen, R. Rolfes, and M. Köntges, "Fracture Probability, Crack Patterns, and Crack Widths of Multi crystalline Silicon Solar Cells in PV Modules During Mechanical Loading," IEEE Journal of Photovoltaics, vol. 8, no. 6, pp. 1510-1524, Nov. 2018.
2. M. Dhimish and P. Mather, "Development of Novel Solar Cell Micro Crack Detection Technique," IEEE Transactions on Semiconductor Manufacturing, vol. 32, no. 3, pp. 277-285, Aug. 2019.
3. P. Mather and M. Dhimish, "Ultrafast High-Resolution Solar Cell Cracks Detection Process," IEEE Transactions on Industrial Informatics, vol. 16, no. 7, pp. 4769-4777, Jul. 2020.
4. B. Su, H. Chen, Y. Zhu, W. Liu, and K. Liu, "Classification of manufacturing defects in multicrystalline solar cells with novel feature descriptor," IEEE Trans. Instrum. Meas., vol. 68, no. 12, pp. 4675–4688, Dec. 2021.
5. M. R. U. Rahman and H. Chen, "Defects Inspection in Polycrystalline Solar Cells Electroluminescence Images Using Deep Learning," IEEE Access, vol. 8, pp. 40547-40558, 2020.
6. R. Duru et al., "Photoluminescence Imaging for Buried Defects Detection in Silicon: Assessment and Use-Cases," IEEE Transactions on Semiconductor Manufacturing, vol. 32, no. 1, pp. 23-30, Feb. 2019.
7. Y. Zhu, F. D. Heinz, M. Juhl, M. C. Schubert, T. Trupke, and Z. Hameiri, "Photoluminescence Imaging at Uniform Excess Carrier Density Using Adaptive Nonuniform Excitation," IEEE Journal of Photovoltaics, vol. 8, no. 6, pp. 1787-1792, Nov. 2018.
8. M. Dhimish, "Thermal impact on the performance ratio of photovoltaic systems: A case study of 8000 photovoltaic installations," in Case Studies in Thermal Engineering, vol. 21, pp. 100693, Oct. 2020.
9. M. Seyedmahmoudian, T. K. Soon, B. Horan, A. Ghandhari, S. Mekhilef, and A. Stojcevski, "New ARMO-based MPPT Technique to Minimize Tracking Time and Fluctuation at Output of PV Systems under Rapidly Changing Shading Conditions," IEEE Transactions on Industrial Informatics, 2019, vol.1, pp.1-10.
10. S. Deitsch et al., "Automatic classification of defective photovoltaic module cells in electroluminescence images," Sol. Energy, vol. 185, pp. 455–468, 2019.
11. H. Y. Chen et al., "Solar cell surface defect inspection based on multispectral convolutional neural network," J. Intell. Manuf., vol. 31, no. 2, pp. 453–468, Feb. 2020.
12. J. M. Greulich et al., "Comparison of Inline Crack Detection Systems for Multicrystalline Silicon Solar Cells," in IEEE Journal of Photovoltaics, vol. 10, no. 5, pp. 1389-1395, Sept. 2020.

13. Mahmoud Dhimish, Violeta Holmes, “Solar cells micro crack detection technique using state-of-the-art electroluminescence imaging”, Journal of Science: Advanced Materials and Devices 4 (2019), pp. 499-508.
14. Akash Singh Chaudhary, D.K.Chaturvedi, “Analyzing Defects of Solar Panels under Natural Atmospheric Conditions with Thermal Image Processing”, I.J. Image, Graphics and Signal Processing, 2018, 6, pp. 10-21.
15. Mira Hayati , Kahlil Muchtar , Roslidar , Novi Maulina , Irfan Syamsuddin, “Impact of CLAHE-based image enhancement for diabetic retinopathy classification through deep learning”,Procedia Computer Science, Volume 216, 2023, Pages 57-66.
16. M. R. Islam and A. Matin, "Detection of COVID 19 from CT Image by The Novel LeNet-5 CNN Architecture," 2020 23rd International Conference on Computer and Information Technology (ICCIT), DHAKA, Bangladesh, 2020, pp. 1-5.
17. Inderpreet Singh, Gulshan Goyal, Anmol Chandel, “AlexNet architecture based convolutional neural network for toxic comments classification”, Journal of King Saud University - Computer and Information Sciences, Volume 34, Issue 9, October 2022, Pages 7547-7558.
18. M. Swapna, Yogesh Kumar Sharma, B M G Prasadh, “CNN Architectures: Alex Net, Le Net, VGG, Google Net, Res Net”, International Journal of Recent Technology and Engineering (IJRTE), Volume-8 Issue-6, March 2020.
19. Vimala, M., Ramadas, G., Perarasi, M., Manokar, A. M., & Sathyamurthy, R. (2023). A review of different types of solar cell materials employed in bifacial solar photovoltaic panel. *Energies*, *16*(8), 3605.
20. Ramadas, G. (2022). Detection of cracks in solar panel images using complex wavelet transform and anfis classification method.
21. Perarasi, M., &Ramadas, G. (2023). Detection of Cracks in Solar Panel Images Using Improved AlexNet Classification Method. *Russian Journal of Nondestructive Testing*, *59*(2), 251-263.
22. Subramanian, K., Meenakshisundaram, N., & Barmavatu, P. (2024). Experimental and theoretical investigation to optimize the performance of solar still. *Desalination and Water Treatment*, *318*, 100343.
23. Subramanian, K., Meenakshisundaram, N., Barmavatu, P., & Govindarajan, B. (2024). Experimental investigation on the effect of nano-enhanced phase change materials on the thermal performance of single slope solar still. *Desalination and Water Treatment*, *319*, 100416.
24. Raju, R. U., Kottala, R. K., Varma, B. M., Krishna, P., & Barmavatu, P. (2024). Internet of Things and hybrid models-based interpretation systems for surface roughness estimation. *AI EDAM*, *38*, e11.
25. Anvari, Z., & Athitsos, V. (2021). A survey on deep learning based document image enhancement. *arXiv preprint arXiv:2112.02719*.
26. Razzak, M. I., Naz, S., & Zaib, A. (2017). Deep learning for medical image processing: Overview, challenges and the future. *Classification in BioApps: Automation of decision making*, 323-350.